

# Nanoscale

Accepted Manuscript



This is an *Accepted Manuscript*, which has been through the Royal Society of Chemistry peer review process and has been accepted for publication.

*Accepted Manuscripts* are published online shortly after acceptance, before technical editing, formatting and proof reading. Using this free service, authors can make their results available to the community, in citable form, before we publish the edited article. We will replace this *Accepted Manuscript* with the edited and formatted *Advance Article* as soon as it is available.

You can find more information about *Accepted Manuscripts* in the [Information for Authors](#).

Please note that technical editing may introduce minor changes to the text and/or graphics, which may alter content. The journal's standard [Terms & Conditions](#) and the [Ethical guidelines](#) still apply. In no event shall the Royal Society of Chemistry be held responsible for any errors or omissions in this *Accepted Manuscript* or any consequences arising from the use of any information it contains.



Journal Name

ARTICLE

## Raman selection rule of surface optical phonon in ZnS nanobelts

Chih-Hsiang Ho,<sup>a,b</sup> Purushothaman Varadhan,<sup>a</sup> Hsin-Hua Wang,<sup>a</sup> Cheng-Ying Chen,<sup>a</sup> Xiaosheng Fang,<sup>c</sup> and Jr-Hau He<sup>\*a</sup>

Received 00th January 20xx,  
Accepted 00th January 20xx

DOI: 10.1039/x0xx00000x

www.rsc.org/

We report Raman scattering results of high-quality wurtzite ZnS nanobelts (NBs) grown by chemical vapor deposition. In Raman spectrum, the ensembles of ZnS NBs exhibit first order phonon modes at 274  $\text{cm}^{-1}$  and 350  $\text{cm}^{-1}$ , corresponding to  $A_1/E_1$  transverse optical and  $A_1/E_1$  longitudinal optical phonons, in addition with strong surface optical (SO) phonon mode at 329  $\text{cm}^{-1}$ . The existence of SO band is confirmed by its shift with different surrounding dielectric media. Polarization dependent Raman spectrum was performed on a single ZnS NB and for the first time SO phonon band has been detected on a single nanobelt. Different selection rules of SO phonon mode shown from their corresponding  $E_1/A_1$  phonon modes were attributed to the anisotropic translational symmetry breaking on the NB surface.

### Introduction

Semiconducting nanomaterials provide new opportunities to exploit distinct properties from their bulk counterparts, making them as the potential candidates for near future electronic and optoelectronic applications.<sup>1-3</sup> These distinct properties not only bring possible breakthrough on device applications but also come with unique physical phenomenon. For example, large surface-to-volume ratio and local surface modulation of nanomaterials, leads to the observation of extraordinary phonon mode known as surface optical (SO) phonon mode, which is not observed for their bulk counterparts.<sup>4</sup> Raman scattering a non-destructive tool often used to investigate material properties such as composition or strain, has also been used to detect the SO phonon modes. Raman scattering has been employed to detect the SO phonon mode in various semiconductor nanostructures, including ZnS, ZnO, CdSe, GaP, GaAs and GaN.<sup>4-12</sup> However, an essential property of Raman scattering, the selection rule for the SO phonon mode has not been widely observed for the single nanostructures, because of the poor signal to noise ratio and weak SO band as compared to their corresponding first order bands.

In this paper, we report the selection rule of Raman scattering for SO phonon modes in ZnS nanobelts (NBs) by polarization dependent Raman spectrum. The surface phonon mode in Raman spectrum was usually observed for an ensemble of nanostructures. Here, in order to understand the

selection rule, we performed the Raman scattering measurements on a single ZnS NB and successfully observed the SO phonon mode, which to the best of our knowledge, has never been seen in previous literatures. The selection rule of SO phonon mode was then found to be broken by the anisotropic translation symmetry breaking on the surface.

### Experimental Section

The ZnS NBs were grown by simple chemical vapor deposition method.<sup>13</sup> High pure ZnS powder (99.999%) and argon (Ar) gas was used as the source material and carrier gas respectively. ZnS powder was placed in an alumina boat and inserted into the center of the quartz tube. A Si wafer with 3 nm Au pre-deposited was placed at the downstream of the ZnS source. After purging the tube by Ar at 500 sccm (standard cubic center per minute), the furnace was ramped to 1100 °C and kept constant at this temperature for 30 minutes. After growth, the furnace was cooled down, with continuous flow of Ar.

The structural properties of as-grown ZnS NBs were characterized by x-ray diffraction, scanning electron microscopy (SEM), transmission electron microscopy (TEM) and Micro-Raman scattering. Micro-Raman scattering measurements were performed in backscattering geometry using Jobin Yvon T6400 Raman spectrometer with a resolution of 0.3  $\text{cm}^{-1}$ . The wavelength of 532 nm laser was used as an excitation source and the laser beam was focused through a microscope with a spot size of about 1  $\mu\text{m}$  in diameter. The typical laser power at the surface of NBs was 4 mW. A liquid nitrogen cooled charge coupled device was used to collect the scattered signal dispersed on 1800 grooves/mm grating. For Raman measurements of a single ZnS NB, the as-grown ZnS NBs on Si were sonicated in alcohol and dispersed on glass substrates.

<sup>a</sup> Computer, Electrical and Mathematical Sciences and Engineering (CEMSE) Division, King Abdullah University of Science & Technology (KAUST), Thuwal 23955-6900, Saudi Arabia Email: [jrhau.he@kaust.edu.sa](mailto:jrhau.he@kaust.edu.sa)

<sup>b</sup> Electrical and Computer Engineering, Purdue University, West Lafayette, IN 47907, USA

<sup>c</sup> Department of Materials Science, Fudan University, Shanghai 200433, P. R. China

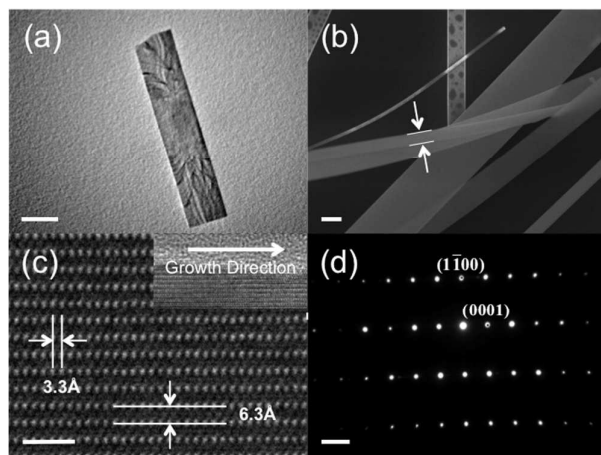


Fig. 1 (a) TEM image, (b) cross-sectional SEM image, (c) HRTEM image and (d) SAED of as-grown ZnS NBs. The scale bar is 0.5  $\mu\text{m}$  for (a) and (b) and 2 nm for (c) and (d), respectively.

## Results and discussion:

Figure 1a shows the TEM image of the ZnS NBs dispersed on copper grid and Fig. 1b shows the SEM image of ZnS NBs dispersed on Si substrates. As grown nanostructures have belt-like morphology with the typical dimension of 0.5  $\mu\text{m}$  in width and 50 nm in thickness. The length of the NBs varies up to few tens of micrometers. Figure 1(c) shows the high resolution TEM (HRTEM) image with clearly resolved lattice arrangements, indicating high crystal quality of the as-grown ZnS NBs. The inset of Fig. 1(c) shows that the ZnS NBs are grown along  $(1\bar{1}00)$  direction and the inter-planar spacing values are found to be 3.3  $\text{\AA}$  and 6.3  $\text{\AA}$  corresponding to  $(1\bar{1}00)$  and  $(0001)$  crystal plane of wurtzite ZnS, which are close to the lattice constant of bulk wurtzite ZnS.<sup>14</sup> The selective area electron diffraction (SAED) also shows diffraction pattern with sharp fringe, confirming the high crystal quality of the ZnS NBs.

Wurtzite ZnS belongs to the space group  $C_{6v}^3$  with two formula units per unit cell. As conventional group theory predicts, the wurtzite structure has several phonon modes including  $A_1$ ,  $E_1$ ,  $E_2$  and  $B_1$ .  $A_1$  and  $E_1$  modes are both Raman and infrared spectra active,  $E_2$  modes are Raman active and  $B_1$  modes are optically silent. The  $A_1$  phonon mode polarizes along  $c$ -axis of wurtzite structure while the  $E_1$  mode polarizes perpendicular to the  $c$ -axis.<sup>15, 16</sup> For wurtzite ZnS,  $A_1$  and  $E_1$  modes are reported to be nearly overlapped, which could be attributed to small anisotropy of inter-atomic force in ZnS.<sup>17</sup> Other than this, due to small Bohr radius around 2.5 nm of ZnS, phonon confinement effect is not expected in our ZnS NBs.<sup>18</sup>

The Raman spectrum collected from an ensemble of ZnS NBs is shown in Fig. 2. Each of the phonon wavenumbers is extracted by fitting the spectrum to a Lorentzian line shape. The peak at 350  $\text{cm}^{-1}$  can be assigned to the  $E_1/A_1(\text{LO})$  mode

and the peak at 274  $\text{cm}^{-1}$  can be assigned to the  $E_1/A_1(\text{TO})$  mode.<sup>5</sup> The broad features at 350~450  $\text{cm}^{-1}$  are related to the second-order Raman scattering, including combination and overtone of several ZnS phonon modes. The peak position of the ZnS bulk phonon modes is close to the reported bulk values, indicating the excellent crystal quality with strain-free growth of ZnS NBs.<sup>5</sup> The SO phonon modes are observed at 329  $\text{cm}^{-1}$  with stronger intensity than its corresponding  $E_1/A_1(\text{LO})$  modes, which has been attributed to the high surface-to-volume ratio of the ZnS NBs. Note that SO phonon modes are usually weaker than related bulk modes and appear as a shoulder band.<sup>4,6,19</sup> However, in our case the SO phonon mode for ensemble of NBs is stronger than LO and TO modes, encouraging us to investigate the SO phonon band in a single ZnS NB.

The SO phonon mode originates from the existence of an interface between materials with different dielectric constants ( $\epsilon$ ). The essential properties of SO phonon modes are that their peak position and line shape depends on the dielectric medium in contact with the surface. SO phonon modes have to be activated by symmetry breaking mechanism associated with the modulation in the surface. It propagates along the interface and has amplitude decays exponentially into the bulk.<sup>20</sup> At the interface, the translational symmetry is broken due to surface roughness or geometrical dimension fluctuation made intentionally or unintentionally during growth process.<sup>4,6,21,22</sup> The translational symmetry breaking gives additional crystal momentum that allows the transition of phonon mode away from the center of the Brillouin zone, which is not allowed in bulk material with perfect crystal symmetry due to momentum conservation. Therefore, nanomaterials with a large surface area provide much stronger SO phonon signal compared to the bulk phonon mode.

According to the dielectric continuum model, the dispersion relation of the phonon mode at the interface will be changed due to different  $\epsilon$ 's of surrounding materials.<sup>5,23</sup> As a result, the wavenumber of SO phonon mode ( $\omega_{\text{SO}}$ ) changes with  $\epsilon$ 's of the surrounding materials.

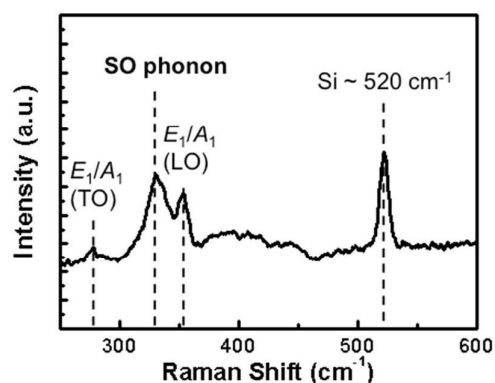


Fig. 2 Raman spectrum from an ensemble of ZnS NBs on Si substrate. The peak at 520  $\text{cm}^{-1}$  has been attributed to Si.

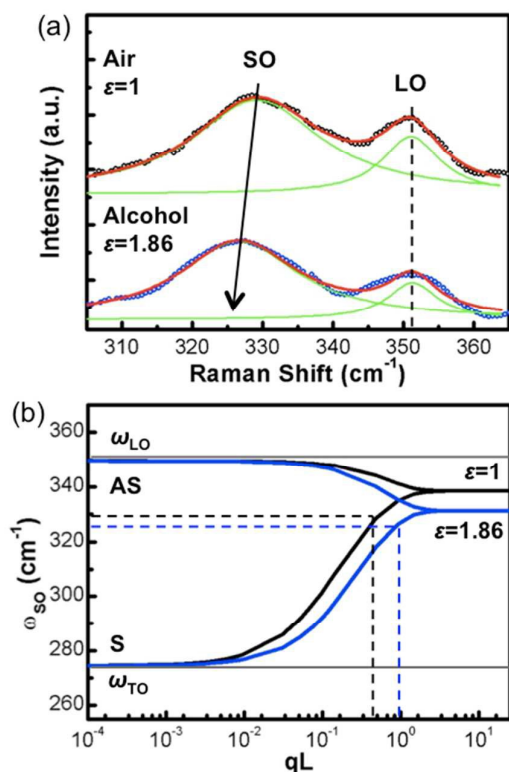


Fig. 3 (a) Raman spectra measured in surrounding material with different dielectric constants (air and alcohol); (b) Calculated SO phonon dispersion relation in air and alcohol.  $q_i L_i$  is (the phonon wavevector)\*(the feature size of the ZnS NBs).

To confirm the existence of SO phonon mode in the ZnS NBs, we compared the Raman spectra of samples immersed in air ( $\epsilon=1$ ) and alcohol ( $\epsilon=1.86$ ). As shown in Fig. 3a,  $\omega_{SO}$  blue-shifts from  $329 \text{ cm}^{-1}$  to  $326 \text{ cm}^{-1}$  when immersed in alcohol while the bulk mode  $E_1/A_1$ (LO) remains the same value at  $351 \text{ cm}^{-1}$ . This result validates the assignment of the SO phonon mode at  $329 \text{ cm}^{-1}$ , demonstrating the surface-related characteristics of SO phonon mode.

To further understand how the surface phonon mode is affected by the surrounding material, we employed the calculation describing the dispersion relation of SO phonon mode in ZnS NBs as an extreme case of rectangular quantum wire.<sup>23</sup> Note that the calculation neglects the potential function describing the optical phonon mode at the corner and assumed the potential function is separable. By utilizing the electrostatic boundary condition, the dispersion relation of SO phonon is derived as below:

$$\epsilon(\omega) \times \tanh(q_i L_i / 2) + \epsilon_s = 0, \quad (1)$$

$$\epsilon(\omega) \times \coth(q_i L_i / 2) + \epsilon_s = 0, \quad (2)$$

where  $\epsilon(\omega)$  and  $\epsilon_s$  are the dielectric constant of ZnS NBs and the surrounding material, respectively,  $\omega$  is the related phonon wavenumber,  $q_i$  is the phonon wavevector and  $L_i$  is the feature size of the ZnS NBs. Equation (1) is the symmetric (S) mode and equation (2) is the antisymmetric (AS) mode. By combining together the dielectric function and the Lyddane-Sachs-Teller relation, we obtained the following dispersion relations of SO phonon mode<sup>5</sup>:

$$\omega_{SO}^2(q)_s = \omega_{LO}^2 \times \left[ \frac{\epsilon_\infty \times (\epsilon_0 \tanh(q_i L_i / 2) + \epsilon_s)}{\epsilon_0 \times (\epsilon_\infty \tanh(q_i L_i / 2) + \epsilon_s)} \right], \quad (3)$$

$$\omega_{SO}^2(q)_{AS} = \omega_{LO}^2 \times \left[ \frac{\epsilon_\infty \times (\epsilon_0 \coth(q_i L_i / 2) + \epsilon_s)}{\epsilon_0 \times (\epsilon_\infty \coth(q_i L_i / 2) + \epsilon_s)} \right], \quad (4)$$

where  $\epsilon_0$  and  $\epsilon_\infty$  are low and high frequency values of  $\epsilon(\omega)$ . Based on these equations, we have calculated the dispersion relation of the SO phonon mode of ZnS NBs in air and alcohol as shown in Fig. 3b. In alcohol, the dispersion relation shifts to lower frequency at the region of higher crystal momentum and remains unchanged at the zone center of the Brillouin zone. The corresponding experimental  $\omega_{SO}$  (Fig. 3a) in alcohol and air are labeled by the horizontal arrow and found to intersect with the S mode branch, indicating SO phonon is in transverse mode. In accordance with the calculated dispersion relation,  $\omega_{SO}$  is observed to shift to lower frequency while the slight difference in wavevector  $q_i$  is attributed to the different spot that the Raman spectra was collected. It is also worth to mention that for SO phonon in transverse mode with given wavevector  $q_i$ , larger feature size  $L_i$ , which denotes the direction SO phonon vibrates, leads to higher  $\omega_{SO}$ .

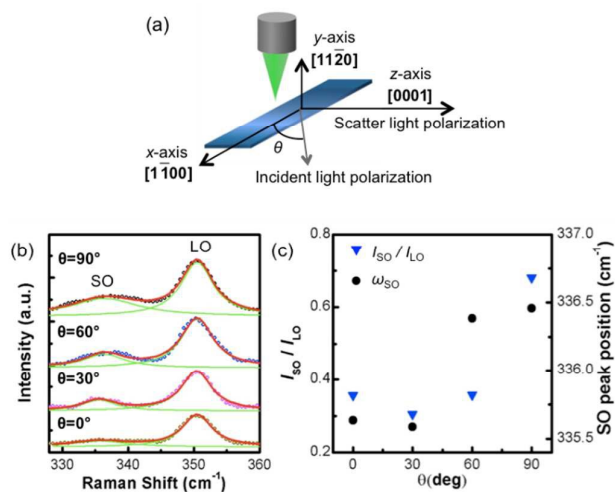


Fig. 4 (a) Schematic illustration of the polarization dependent Raman measurement. (b) Polarization dependent Raman spectra measured from a single ZnS NB with different angles. (c) angular dependency of  $I_{LO} / I_{SO}$  and  $\omega_{SO}$ . Single ZnS NB with different angles. (c) angular dependency of  $I_{LO} / I_{SO}$  and  $\omega_{SO}$ .

To gain insight into the selection rule of SO phonon mode of ZnS nanostructures, we measured the polarization-dependent Raman spectrum of a single ZnS NB and the experimental setup is schematically shown in Fig. 4a. The polarization of incident light was varied from  $x$  to  $z$  direction while only the scattered light polarized in  $z$  direction was collected. More specifically, the light configuration was changed from  $Y(X,Z)$ - to  $Y(Z,Z)$ -. The angle  $\theta$  is defined as the angle between  $x$  axis and scattering polarization is changed from  $0^\circ$  to  $90^\circ$ . The polarization-dependent Raman spectra with four different angles are shown in Fig. 4b. The intensities of LO and SO phonon modes increase as the incident laser polarization changes from  $x$  direction to  $z$  direction.

The intensity ratio  $I_{SO}/I_{LO}$  as a function of  $\theta$  is found to increase from 0.35 to 0.68 as  $\theta$  changes from  $0^\circ$  to  $90^\circ$  (Fig. 4c). The peculiar difference in  $I_{SO}/I_{LO}$  with  $\theta$  indicates that SO and LO phonon have different selection rules, which is not expected because SO phonon mode originates from exactly the same atomic vibration with LO phonon modes even as  $\theta$  changes. The selection rule that describes the polarization dependency of Raman scattering shows that the intensity of Raman scattering can be expressed as:

$$I \propto |\vec{e}_s \times \vec{R} \times \vec{e}_i|^2 \quad (5)$$

where  $I$  is the intensity,  $\vec{e}_s$  and  $\vec{e}_i$  are the polarization vectors of scattering light and incident light, respectively, and  $\vec{R}$  is the Raman tensor. The Raman tensor of two vibration modes,  $A_1$  and  $E_1$  modes, of LO phonon can be expressed as<sup>15</sup>

$$E_1(x) = \begin{bmatrix} 0 & 0 & c \\ 0 & 0 & 0 \\ c & 0 & 0 \end{bmatrix} \quad (6)$$

$$A_1(z) = \begin{bmatrix} a & 0 & 0 \\ 0 & a & 0 \\ 0 & 0 & b \end{bmatrix} \quad (7)$$

where  $a$ ,  $b$ , and  $c$  are constants related to electric polarizability. In this case, we have  $\vec{e}_s = \hat{z}$  and  $\vec{e}_i = \cos \theta \hat{x} + \sin \theta \hat{z}$ , where  $\hat{x}$  and  $\hat{z}$  are the unit vectors along  $x$ -axis and  $z$ -axis as shown in Fig. 4a, respectively. The total intensity of LO phonon mode ( $I_{LO}$ ) can be derived as

$$I_{LO} = I_{A_1} + I_{E_1} = b^2 \sin^2 \theta + c^2 \cos^2 \theta = y_0 + a_0 \sin^2 \theta,$$

where  $y_0$  and  $a_0$  are constants. As light configuration varies from  $Y(X,Z)$ - to  $Y(Z,Z)$ -, the allowed phonon mode is changed from  $E_1$  to  $A_1$  while the total intensity varies with  $\sin^2 \theta$ , explaining the change of  $I_{LO}$  with  $\theta$ . However, SO phonon mode having the same vibration modes doesn't have the same selection rule so that  $I_{SO}$  becomes much stronger for  $Y(Z,Z)$ - than  $I_{LO}$ , indicating  $A_1$  vibration mode is amplified for SO phonon. During the growth of NBs, growth condition in local

regime continuously changes over time, inducing periodic surface roughness in the NB. As a result, surface roughening-induced translation symmetry breaking mostly occurs in growth direction, which is  $x$ -axis in our case.<sup>4-6,21,22</sup> Accordingly, we suggest that SO phonon modes is dominated by phonon mode propagating along  $x$ -axis, which is  $A_1(\text{TO})$  in this case. This inference is in accordance with our calculated results as shown in Fig. 3b, that the SO phonon modes are in transverse mode. Moreover, the feature size  $L_x$  of  $A_1(\text{TO})$  mode is several  $\mu\text{m}$  larger than the feature size  $L_z$  of  $E_1(\text{TO})$  mode, which is around 500 nm. Therefore, according to the calculated dispersion relation in Fig. 3c, SO phonon mode related to  $A_1(\text{TO})$  vibration mode would have larger  $qL_z$  that leads to higher  $\omega_{SO}$  compared to SO phonon mode related to  $E_1(\text{TO})$ , which is in agreement with the variation of  $\omega_{SO}$  as shown in Fig. 4c.

## Conclusions

Wurtzite ZnS NBs with high crystalline quality were grown by the chemical vapor deposition. From Raman scattering measurements, we have observed strong SO phonon mode in the ZnS NBs. The phonon wavenumber  $\omega_{SO}$  is found to blue-shifted as the dielectric constant of surrounding material increases, confirming the presence of SO phonon mode, which is in accordance with the calculation. Based on the polarization dependent Raman spectrum of a single ZnS NB, the selection rule of SO phonon is broken. The  $A_1(\text{TO})$  related SO phonon mode was found to dominate over  $E_1$  related SO phonon mode, which has been attributed to the anisotropy in translational symmetry breaking condition brought by the feature of nanostructure growth.

## Acknowledgements

This research was supported by King Abdullah University of Science and Technology (KAUST) baseline funding.

## Notes and references

1. Y. Huang, X. F. Duan and C. M. Lieber, *Small*, 2005, **1**, 142-147.
2. R. Agarwal and C. M. Lieber, *Appl Phys a-Mater*, 2006, **85**, 209-215.
3. X. F. Duan, Y. Huang, R. Agarwal and C. M. Lieber, *Nature*, 2003, **421**, 241-245.
4. R. Gupta, Q. Xiong, G. D. Mahan and P. C. Eklund, *Nano Letters*, 2003, **3**, 1745-1750.
5. Q. H. Xiong, J. G. Wang, O. Reese, L. C. L. Y. Voon and P. C. Eklund, *Nano Lett*, 2004, **4**, 1991-1996.
6. S. Bhattacharya, A. Datta, S. Dhara and D. Chakravorty, *J Raman Spectrosc*, 2011, **42**, 429-433.
7. Y. F. Huang, S. Chattopadhyay, H. C. Hsu, C. T. Wu, K. H. Chen and L. C. Chen, *Opt Mater Express*, 2011, **1**, 535-542.
8. D. Fan, R. Zhang, Y. Zhu and H. Peng, *Physica B: Condensed Matter*, 2012, **407**, 3510-3514.
9. R. Mata, A. Cros, K. Hestroffer and B. Daudin, *Physical Review B*, 2012, **85**, 035322.

10. I. M. Tiginyanu, A. Sarua, G. Irmer, J. Monecke, S. M. Hubbard, D. Pavlidis and V. Valiaev, *Physical Review B*, 2001, **64**, 233317.
11. G. D. Mahan, R. Gupta, Q. Xiong, C. K. Adu and P. C. Eklund, *Physical Review B*, 2003, **68**, 073402.
12. H. Lange, M. Artemyev, U. Woggon and C. Thomsen, *Nanotechnology*, 2009, **20**, 045705.
13. Q. Li and C. R. Wang, *Appl Phys Lett*, 2003, **83**, 359-361.
14. JCPDS, *Journal*, 1967.
15. C. A. Arguello, D. L. Rousseau and S. P. S. Porto, *Phys Rev*, 1969, **181**, 1351.
16. H. Harima, *J Phys-Condens Mat*, 2002, **14**, R967-R993.
17. R. Loudon, *Advances in Physics*, 1964, **13**, 423-482.
18. R. Rossetti, R. Hull, J. M. Gibson and L. E. Brus, *J Chem Phys*, 1985, **82**, 552-559.
19. D. Spirkoska, G. Abstreiter and A. F. I. Morral, *Nanotechnology*, 2008, **19**, 435704.
20. K. W. Adu, Q. Xiong, H. R. Gutierrez, G. Chen and P. C. Eklund, *Appl Phys A-Mater*, 2006, **85**, 287-297.
21. S. Sahoo, S. Dhara, A. K. Arora, R. Krishnan, P. Chandramohan and M. P. Srinivasan, *Applied Physics Letters*, 2010, **96**, 103113-103113.
22. J. H. Zhu, J. Q. Ning, C. C. Zheng, S. J. Xu, S. M. Zhang and H. Yang, *Applied Physics Letters*, 2011, **99**, 113115-113113.
23. M. A. Stroschio, K. W. Kim, M. A. Littlejohn and H. H. Chuang, *Physical Review B*, 1990, **42**, 1488-1491.